Alpha-Cluster Structures in Medium Light Nuclei

Markus Norrby

Physics
Department of Natural Sciences
Åbo Akademi University

Åbo 2011

Supervisor:

Docent Tom Lönnroth
Åbo Akademi University

Pre-examiners:

Professor Joakim Cederkäll
University of Lund

Professor Rauno Julin
University of Jyväskylä

Opponent for the public defense:

Dr David Jenkins
University of York

ISBN 978-952-12-2659-5

Painosalama – Åbo 2011

Acknowledgements

The book you now hold in your hand is the result of about five years of full-time, part-time and free-time research work. I have had the privilege of working at my own pace with flexible arrangements, as the conditions of Life has changed over the years.

I would like to express my warmest thanks to the whole physics team at the Department of Natural Sciences at Åbo Akademi University. Most of all naturally to my wonderfully positive supervisor Tom Lönnroth, but also to Ronald Österbacka, Mårten Brenner, Kjell-Mikael Källman and all the other staff and students who all helped make this project possible and fun to do.

I am also very grateful for the patient guidance and help of Vladilen Goldberg at Texas A&M University and Grigory Rogachev at Florida State University, as well as their respective colleagues who helped in making my visits to these institutions fruitful and interesting. Additionally, the generous grants awarded by Stiftelsens för Åbo Akademi forskningsinstitut, Magnus Ehrnroots stiftelse, Svenska kulturfonden and Svenska Tekniska Vetenskapsakademien have been very appreciated.

The support from my beloved family and dear friends has been invaluable, but the biggest thank you of all goes to my fabulous wife Jenny who has put up with me and cheered me on throughout this process. I love you honey!

Vasa
August 29th, 2011

Svensk sammanfattning

Trots att kärnfysiken varit ett av de mest framgångsrika vetenskapsområdena de senaste hundra åren döljer atomkärnan fortsättningsvis många mysterier. Det finns fortfarande ingen heltäckande teori som beskriver de kända isotopernas kärnegenskaper. För de allra lättaste grundämnena har stora framsteg gjorts de senaste åren med hjälp av komplicerade datorberäkningar, men fastän datorerna skulle fortsätta utvecklas lika snabbt som idag så dröjer det ändå tiotals, kanske hundratals år, innan världens datorkraft räcker till för att utföra dessa beräkningar för tyngre element. Tills vidare behövs ett lappverk av olika modeller för att vi ska kunna förstå de egenskaper vi observerar hos atomkärnor, och i detta lappverk är klustermodeller en viktig bit.

Att neutroner och protoner i en atomkärna i vissa fall kunde ”klumpa ihop sig” till alfapartiklar (bestående av två protoner och två neutroner) förutsågs redan 1938 av L. R. Hafstad och E. Teller. Detta har entydigt observerats i de lättaste isotoperna som kan byggas upp av uteslutande alfapartiklar, till exempel ^{8}Be och ^{12}C. Dessa så kallade alfakluster förväntas också formas i tyngre kärnor, men i de tyngre kärnorna finns betydligt fler energitillstånd, och på grund av de kvantmekaniska kopplingarna mellan dessa blir bilden allt mer komplicerad. På senare tid har både teoretiska och experimentella undersökningar visat att alfakluster inte bara kan förekomma i kärnor som består av uteslutande alfapartiklar, utan man kan också addera neutronpar till dessa och fortfarande se klusterstrukturer, och ibland kan extra neutroner till och med framhäva effekten.

Denna avhandling koncentrerar sig på experimentella undersökningar av kärnorna hos de medellätta isotoperna ^{32}S, ^{34}S och ^{40}Ca. Undersökningarna är utförda med hjälp av en relativt ny experimentell metod som baserar sig på omvänd geometri. I detta fall accelereras de tyngre jonerna mot en spridningskammare fylld med den lättare isotopen i gasform. Till exempel har tillstånd med hög excitationsenergi i ^{32}S undersökts genom spridning av ^{28}Si på ^{4}He-gas. Med hjälp av simuleringar kan händelser som registreras av detektorer vid olika vinklar återskapas i massmedelpunktssystemet och därigenom jämföras med tidigare experiment och teoretiska förutsägelser.

Genom att studera de spridningsspektrum som uppstår kan man välja ut resonanser som sannolikt har en alfaklusterstruktur. En tidskrävande matematisk anpassning av dessa komplicerade spektrum gör att man kan bestämma energier, bredder, styrkor och spinvärden för resonanserna, vilket i sin tur ger en uppfattning om hur tydligt klusteregenskaperna framträder. Undersökningen visar att de tre kärnorna ^{32}S, ^{34}S och ^{40}Ca samtliga uppvisar tydliga alfaklusteregenskaper, och fördelningen av klusterresonanserna tyder på att egenskaperna uppstår då kärnan befinner sig i ett tillstånd med en eller några alfapartiklar som roterar kring en stillastående centraldel. Eventuellt kan denna yteffekt betraktas som ett Bose-Einsteinkondensat av alfapartiklar, eller som en kvantmekanisk virvelström. Ytterligare experimentella och teoretiska undersökningar behövs dock för att klargöra dessa samband.

En genomgång av tillgänglig litteratur visar att det för närvarande finns ett stort intresse för klusterstrukturer i atomkärnor. Den största delen av arbetet bedrivs bland de lätta kärnorna, men det finns också ett ökande intresse för klustereffekter i medellätta, tunga och till och med hypotetiska supertunga kärnor. Bland de medellätta kärnorna finns en hel del experimentellt material som byggts upp under åren, bland annat av kärnfysikgruppen vid Åbo Akademi som under ledning av professor Mårten Brenner började arbeta med dessa frågor för nästan 30 år sedan. De teoretiska förklaringarna släpar tills vidare efter, samtidigt som många oklarheter ännu måste redas ut experimentellt som grund för mer djupgående teoretiska analyser.

Outline

This thesis summarizes recent experimental work performed by the nuclear physics group at Åbo Akademi University together with collaborators. The first chapter gives a motivation for the work and a brief look back at the history of clusters in nuclear physics, as well as a short review of the current state of affairs. Cluster models are a very important complement to other nuclear models. Recent discoveries show that cluster phenomena are very important for a wide variety of nuclear configurations and reactions, also among medium light nuclei with $16 \leq A \leq 44$.

In the second chapter a brief survey of the available experimental techniques for resonance scattering is presented. Traditional approaches using thin targets or transfer reactions are mentioned, but emphasis are on novel thick-target methods, and especially the Thick Target Inverse Kinematics Technique (TTIK) used in the recent experiments. The challenges in constructing an excitation function from the TTIK data as well as the theoretical foundation for the simplified R-matrix analysis used and the details of the fitting procedure are discussed.

The third chapter presents the new experimental data on ^{32}S, ^{34}S and ^{40}Ca. The main results from the three nuclei are presented separately, followed by a comparison between them and a discussion of the general features. A summary is given in the forth and final chapter. The results are discussed and some of the many open questions in the field are stated. Some suggestions for future experimental work are also made. Finally, the published papers on which this thesis is based are given as appendices.

List of Publications and Author's Contribution

This thesis is based on work published in the following papers, reproduced as appendices at the end of the book.

1. *Highly Excited Alpha-Cluster states in* ^{32}S *Studied with the Thick Target Inverse Kinematics Method*
T. Lönnroth, M. Norrby, V.Z. Goldberg, G.V. Rogachev, M.S. Golovkov, K.-M. Källman, M. Lattuada, S.V. Perov, S. Romano, B.B. Skorodumov, G.P. Tiourin, W.H. Trzaska, A. Tumino and A.N. Vorontsov.
Eur. Phys. J. A 46 (1), 5 (2010)
© 2010 Springer Science + Business Media

2. *Highly Excited Alpha-Cluster States in* ^{34}S
M. Norrby, T. Lönnroth, V.Z. Goldberg, G.V. Rogachev, M.S. Golovkov, K.-M. Källman, M. Lattuada, S.V. Perov, S. Romano, B.B. Skorodumov, G.P. Tiourin, W.H. Trzaska, A. Tumino and A.N. Vorontsov.
Eur. Phys. J. A 47 (6), 73 (2011)
© 2011 Springer Science + Business Media

3. *Elastic Alpha-Particle Resonances as Evidence of Clustering at High Excitation in* ^{40}Ca
M. Norrby, T. Lönnroth, V.Z. Goldberg, G.V. Rogachev, M.S. Golovkov, K.-M. Källman, M. Lattuada, S.V. Perov, S. Romano, B.B. Skorodumov, G.P. Tiourin, W.H. Trzaska, A. Tumino and A.N. Vorontsov.
Eur. Phys. J. A 47 (8), 96 (2011)
© 2011 Springer Science + Business Media

4. *Evidence of Rotational Behavior of Alpha-Clusters in* ^{32}S, ^{34}S *and* ^{40}Ca
M. Norrby and T. Lönnroth.
Int. J. Mod. Phys. E 20 (4), 1042 (2011)
© 2011 World Scientific Publishing Company

5. *Alpha Clusters in Medium Light Nuclei: Recent Results and Open Questions*
M. Norrby, M. Brenner, T. Lönnroth and K.-M. Källman.
Int. J. Mod. Phys. E 17 (10), 2019 (2008)
© 2008 World Scientific Publishing Company

The PAPERS 1–4 are closely connected and based on data gathered during a week-long experiment in Jyväskylä in April 2002. The author has performed all the analysis of the data, finding the resonance parameters listed in PAPERS 1–3. Together with the collaborators the author has been active in drawing conclusions based on these findings, and he has performed the necessary calculations and produced the graphs needed to present the results. PAPER 5 is a review article where no new data was analyzed, instead the authors strived to compile results and unanswered questions found recently by the Åbo Akademi University nuclear physics group.

In all cases the author wrote the manuscript drafts before finalizing the details together with the respective collaborators. The experiments in Jyväskylä were carried out by a large group of scientists headed by T. Lönnroth and V.Z. Goldberg without the participation of the author. The conversion of raw data into the formats used in the analysis was mainly performed by G.V. Rogachev and B.B. Skorodumov.

Contents

Chapter 1

Introduction

1.1 Background

Even though nuclear physics is one of the most successful scientific disciplines of the last century, it is still a very exciting field with many interesting questions that remain unanswered. There are three large obstacles when constructing theoretical models in nuclear physics:

- The nucleon-nucleon interaction inside the nucleus is not precisely known. Neither are the three-body, four-body or many-body interactions that often are important.
- The nucleus usually involves too many particles for complete quantum mechanical calculations.
- The nucleus contains too few particles for statistical methods to be accurate.

Nuclear models can be categorized on a sliding scale between two extremes. At one end we have the *microscopic models* that use actual, but not precisely known, nucleon-nucleon interactions to solve the Schrödinger equation. This field has made large advances in the last decade or so as computing power has increased. The so called *ab initio* calculations [1] are quite successful for the lightest elements. But due to

the enormous complexity of the calculations, expanding these models to encompass elements heavier than the 13–14 nucleons presently being explored is very slow and highly dependent on available and growing computer power [2]. At the other end of the scale there are the *collective models* [3], like the liquid drop model that ignores the individual features of the nucleons and is able to explain many gross nuclear features, but these models clearly fail to reproduce experimentally observed energy levels in a consistent way.

Most nuclear models are somewhere in between the two extremes mentioned above, for example using a mean field as a potential when solving the Schrödinger equation, instead of the individual interactions. These models are usually tuned to experimental results using free parameters and different models can reproduce most energy levels in different nuclei with good precision. But since none of the models are complete, it often happens that one or a few levels seen experimentally are missing in the predictions made by the models. To be able to explain all the observed levels a combination of different models is often needed.

One important group of nuclear models, especially in the context of this thesis, are the *cluster models* (see e.g. [4, 5, 6, 7]). These models predict that some of the energy levels observed cannot be explained using free nucleons interacting with each other, but rather the nucleons have lumped together into clusters, and it is mainly the clusters that interact with each other.

Here alpha-clusters are especially important because of the special characteristics of the alpha-particle, or ^{4}He nucleus, consisting of two protons and two neutrons. It is tightly bound by 28.3 MeV, compared to only 7.7 MeV for ^{3}He, and has no bound excited states. Early on in nuclear physics it was already predicted that alpha particles might play an important roll in nuclear structure, and this was proven when the alpha-decay of heavy elements was very accurately explained with the model of an alpha-particle forming spontaneously in the nucleus and then tunneling out through the potential barrier [8].

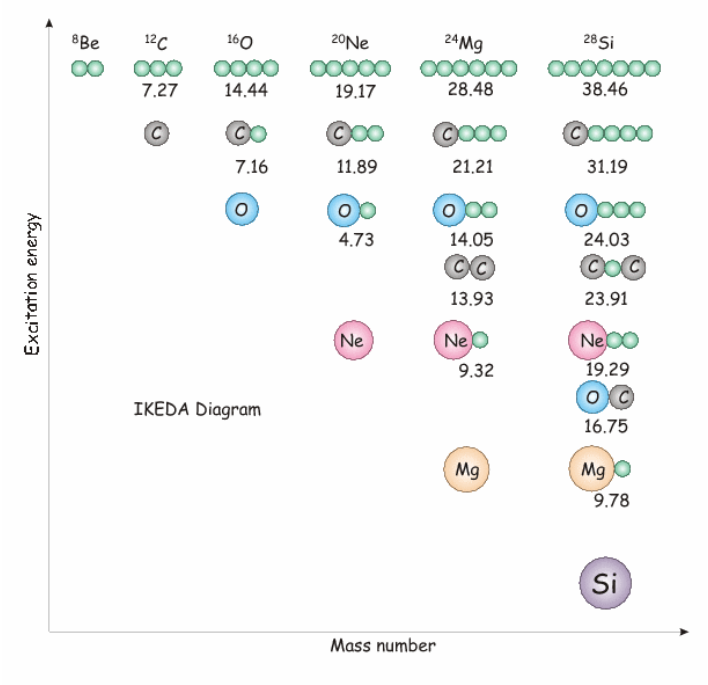

Figure 1.1: The Ikeda diagram as illustrated in [11]. It shows how for example the ^{20}Ne nucleus (the third column from the right) can be viewed as a combination of an ^{16}O nucleus and an alpha-particle, or a ^{12}C nucleus and two alpha particles, or as a cluster of five separate alpha-particles. The numbers below each configuration give the respective break up energies in MeV, and at around these excitation energies the configurations are expected to be observable experimentally.

In the year 1938 Hafstad and Teller published an article titled ”The Alpha-Particle Model of the Nucleus” [9], formulating a simplified theory based on the special properties of the so called alpha-conjugate nuclei, the stable ones being ^{12}C, ^{16}O, ^{20}Ne, ^{24}Mg, ^{28}Si, ^{32}S, ^{36}Ar and ^{40}Ca. The ideas were developed in the following decades and in 1968 Ikeda et al. [10] presented what is now known as the Ikeda diagram (see Figure 1.1 from [11]). In the figure the possible configurations of the alpha-conjugate nuclei are shown, together with the threshold energies for decay into the various channels around which the cluster structures are expected to manifest themselves most clearly.

In recent years a lot of work has been done on extending the picture to non-alpha-conjugate nuclei. By adding neutrons (or in rare cases

protons) the formation of nuclear molecules becomes possible, as has been investigated in some detail by von Oertzen et al. (see e.g. [12]). The valence particles, typically neutrons, can be exchanged between the alpha-particles, providing an attractive force in analogy with the sharing of electrons between atoms in atomic molecules. Some possible configurations are shown in Figure 1.2 from [11].

There are many different forms of cluster interaction in nuclei and cluster phenomena manifest themselves in slightly different ways in different mass regions. Some general observations and recent results are discussed in the following sections.

1.2 Light Nuclei

Among the light nuclei cluster phenomena are well known. These include not only alpha-clusters, but also e.g. ^{3}He and neutron clusters. The nucleus ^{8}Be is unstable and known to have a dumbbell configuration, and it spontaneously breaks up into two alpha-particles with a very short half-life of $6.7 \cdot 10^{-19}$ s. The stable ^{9}Be and semi-stable ^{10}Be ($T_{1/2}$ = $1.5 \cdot 10^{6}$ a) have been found to have strong components of molecular configuration (compare to Figure 1.2). A lot of work is being done at the moment on isotopes of Li, Be and B, especially on the neutron rich isotopes, in order to study molecular states and neutron halos.

The ^{12}C nucleus has been examined in detail from the perspective of alpha-clusters. Indeed, the first excited 0^{+} state in ^{12}C, the so called Hoyle state, is one of the most interesting and most studied individual nuclear states in any nucleus. It has been shown to have a very strong component of three alpha-particles with relatively large spacing between them (see e.g. [13]). Lately theoretical developments have been made describing the state as a Bose-Einstein condensate of three alpha particles in the ground state [14]. An experimental search for an excited Hoyle state is also under way. Some candidates have been found but the results are not yet conclusive. There is also interest in

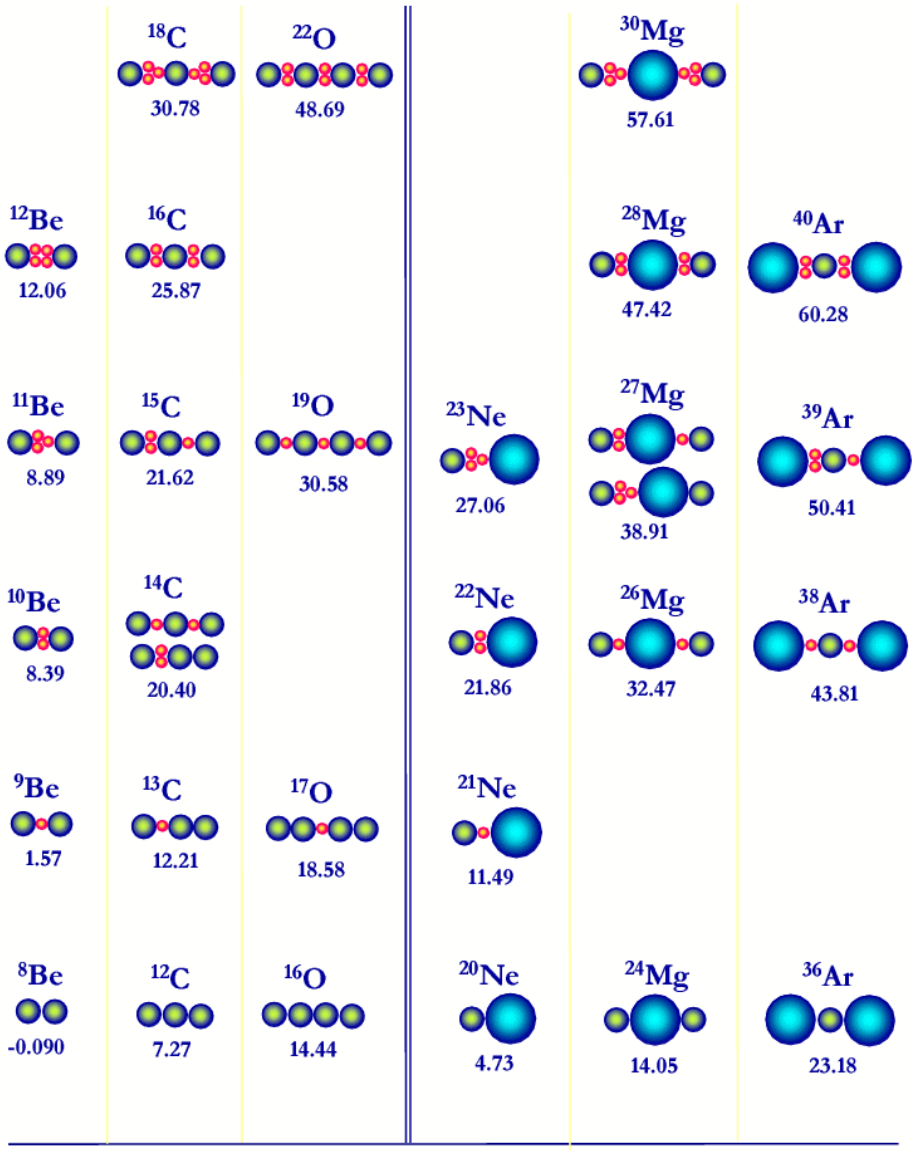

Figure 1.2: Examples of the extended Ikeda diagram as illustrated in [11]. As can be seen the extra neutrons in neutron rich nuclei can form various configurations binding together individual alpha-particles, as in the left panel, or an ^{16}O nuclei and alpha-particles as exemplified in the right panel. Again the threshold energies are given under the illustrations.

examining other isotopes of C in order to see how extra neutrons and neutron-holes affect the cluster structures.

At the moment nuclei involving about 13 nucleons are the heaviest ones possible to simulate through *ab initio* calculations. For heavier systems simplifications must be made, and the comparison between predictions of cluster models and *ab initio* calculations for the light nuclei are of great importance when applying the cluster models in other mass regions.

1.3 Medium Light Nuclei

The nucleus ^{16}O also has strong cluster properties, although not as clear as in ^{12}C. The search is on for a Hoyle state analogue in ^{16}O and some candidates have been found [14]. The ^{18}O isotope has also generated some interest, partly because of the molecular configuration possibilities which do not include a simple molecular chain but instead perhaps an α-particle connected to a molecular configuration in ^{14}C [12].

Basic examinations of the alpha-conjugate nuclei ^{20}Ne, ^{24}Mg and ^{28}Si have been made, but more detailed experiments could and should be done (see e.g. [15, 16]). Many ^{12}C + ^{12}C scattering experiments have also been performed to study states in ^{24}Mg. An interesting experiment was done comparing the alpha-cluster structure of ^{22}Ne and ^{22}Mg [17], both of the type ^{20}Ne$+2n$ and ^{20}Ne$+2p$ respectively. The neutron rich ^{22}Ne showed a very rich structure, while the excitation function for the proton rich ^{22}Mg did not show any clear resonances and no clear analogue states to ^{22}Ne. The rotational cluster bands of ^{22}Ne have recently been further examined in [18]. Otherwise very little data is available on clustering in neutron rich isotopes in this mass region, as discussed in PAPER 2.

The nucleus ^{32}S has been examined in detail in several experiments, reported in e.g. [19, 20, 21, 22, 23] and PAPERS 1 and 5. Many resonances of ^{16}O + ^{16}O experiments have also been associated with cluster states

in ^{32}S, but the relationship between these and observed alpha-cluster states is unclear [24, 25, 26].

Super-deformed bands connected to suggested cluster structures have been found both in ^{36}Ar [27] and in ^{40}Ca [28]. The ^{36}Ar nucleus has been investigated from alpha-cluster point of view for low excitation energy in [29], while data for ^{40}Ca previous to Paper 3 mainly has been gathered for optical potential calculations [30].

The heaviest relatively stable alpha-conjugate nucleus is ^{44}Ti with a half life of 60.4 years. No complete examination of this nucleus has been done, but scattering data show a very rich structure also for ^{44}Ti [31, 32].

1.4 Heavy and Super-Heavy Nuclei

For heavy nuclei the alpha-conjugate isotopes are unstable and experimenting with them is increasingly difficult. The heaviest known alpha-conjugate nucleus is doubly magic ^{100}Sn, and it has generated some interest mainly as a core for various cluster configurations that might help explain the curious α-decay of neutron rich isotopes between ^{105}Te and ^{114}Ba [33]. But there are interesting cluster effects in other types of nuclei as well.

Spontaneous alpha-decay, occurring for nuclei heavier than lead, can be regarded as a special form of alpha-clusterization, where the ground state of the nucleus contains a strong enough admixture of pre-formed alpha-particles for them to tunnel out through the potential barrier with a very reliable decay probability. The mechanisms behind this process are still not completely understood, and it is one of the exciting future applications where the basic research on lighter systems exemplified in this thesis might some day help in understanding the processes inside heavy nuclei. This in turn can perhaps lead to advances in different fields, such as better means of energy production and treatment of nuclear waste through advanced transmutation (e.g. [34]).

In recent years there has been a growing interest in clustering aspects of super-heavy nuclei. An example is the as yet unnamed ^{296}116, which can be seen as a cluster of ^{48}Ca + ^{248}Cm [35]. These kinds of configurations are very important in the reactions where the super-heavies are created, usually in collisions of uranides. There are also theoretical predictions for hollow Fullerene-type structures, especially for isotopes of the element 120, which can be viewed as 60 α-particles and a large number of neutrons stabilizing the structure, culminating in ^{300}120 consisting of two superimposed α_{60} and three n_{60} spheres [36].

So far the emphasis of the people working in this field has been on light nuclear systems and to some extent very heavy systems. But as the cluster models develop, there is a clear need to increase the experimental knowledge of clustering in the medium light nuclei, here defined as nuclei between ^{16}O and ^{44}Ti in the nuclide chart. This thesis gives a synopsis of the recent results on ^{32}S, ^{34}S and ^{40}Ca published by the Åbo Akademi University nuclear physics group, and tries to relate the new findings to what is previously known about clustering in this mass region and in general.

Chapter 2

Experimental Techniques

2.1 Elastic Resonance Scattering as an Experimental Method

Elastic resonance scattering is one of the oldest experimental methods in nuclear physics. By varying the energy of an incident beam of particles and detecting the elastically scattered particles nuclear resonances can be explored. One problem with the method is that all nuclear states are not excited with the same probability, rather the choice of incident nucleus selects different states in the examined highly excited nucleus corresponding to different dominating structure components.

But this can also be used as an advantage when looking for states with a certain structure. For example, scattering alpha-particles off a ^{28}Si nucleus, and detecting the alpha-particles that have not excited the ^{28}Si nucleus (thus, elastic scattering), one expects a rather smooth variation of the intensity of detected alpha-particles depending on the angle of detection. This is simple Rutherford scattering or Coulomb scattering. But if the energy of the incoming alpha-particles is high enough to penetrate the Coulomb barrier, and the energy matches that of an energy level with a suitable configuration in the intermediate nucleus, one expects a resonant effect and a very different pattern where the angular distribution of the scattered particles is governed by the

spin of the resonant level. In the case above the reaction can be written $\alpha + {}^{28}\mathrm{Si} \rightarrow {}^{32}\mathrm{S}^{*} \rightarrow {}^{28}\mathrm{Si} + \alpha$. By finding the energies and widths of the resonances and analyzing the angular distribution of the scattered particles, these parameters can be used to verify if the observed resonances are indeed highly excited and unbound states in the intermediate nucleus with a large percentage of alpha-clusterization.

2.2 The Thin Target Stepping Technique

Elastic scattering of alpha-particles from a very thin target is perhaps the oldest experimental technique of all in nuclear physics, as it was used by Rutherford in the experiments where the atomic nucleus was discovered. In the early experiments natural alpha-particle sources were used, but as different types of accelerators have been developed over the years, it has given physicists very precise control over the energy of the bombarding particles.

A typical experimental setup is shown in Figure 2.1. The particles in the incident beam can pass through the target material without loosing any significant part of their kinetic energy. Coulomb scattering is expected to have its maximum at 0° (along the beam path), while resonant scattering is expected to have its maximum near 180°, so the detectors are usually placed at backward angles, near the beam entrance. The target can be a thin self-supporting film, an element evaporated on a thin backing material, or even a small gas cell.

Using this technique it is very easy to separate the elastic events from inelastic. To create an excitation function, showing the intensity (or cross section) of scattered particles for different energies at a certain angle, the energy of the beam must be varied in small steps, usually 5–50 keV. If the beam is stable and can be varied in small enough steps, the technique can provide data with very high resolution and almost no background disturbances. But in order to examine a large energy interval, say 10 MeV, thousands of steps must be made, taking up weeks or months of valuable beam-time. Therefore the technique is

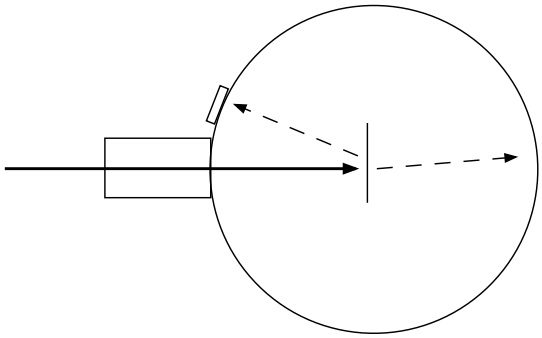

Figure 2.1: The thin target stepping technique uses detectors at backward angles. In most cases the beam particles pass right through the thin target foil, or are only slightly deflected by electromagnetic interaction as illustrated in the figure by the arrow continuing to the right. But if the beam energy matches a nuclear resonance, the incoming particle will interact through the strong interaction with the nucleus and is emitted with enhanced probability at backward angles.

not practical in large-scale investigations.

The shaded area in the main panel of Figure 2.2 shows an example of a spectrum obtained with the thin target stepping technique, at an angle of 173.4° compared to the direction of the beam at the target position. The experiment [19], performed at Florida State University using a Tandem accelerator, scattered alpha particles off a target made by depositing natural silicon on a thin carbon backing. It covers roughly 1 MeV of excitation energy in 5 keV steps, and took about one week to perform. The energy scale is in excitation energy of ^{32}S.

2.3 The Thick Target Backscattering Technique

This technique is similar to the one above, but uses a thicker target as illustrated in Figure 2.3. As the particles of the beam enter the target material, they gradually slow down in the solid target. If an incoming particle interacts with a target nucleus at an energy corresponding to a resonance, it will be backscattered, again slightly slowed down passing back out through the target material, and can be detected at backward angles.

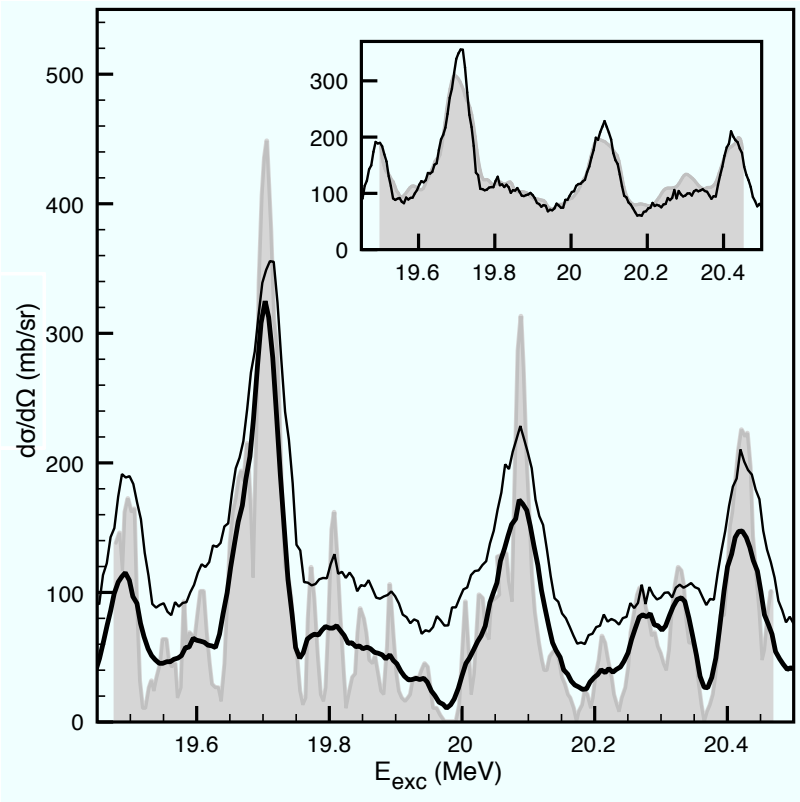

Figure 2.2: Examples of excitation functions from the same region in ^{32}S explored with different experimental methods. The shaded area represents thin target data [19], the thick black line represents thick target data [20] and the thin black line represents data acquired with the thick target inverse kinematics technique (TTIK) from PAPER 1. The insert shows the thin target data smoothed by 45 keV with an additional 50 keV background together with the TTIK data. Note how consistent the data sets are despite the different resolutions.

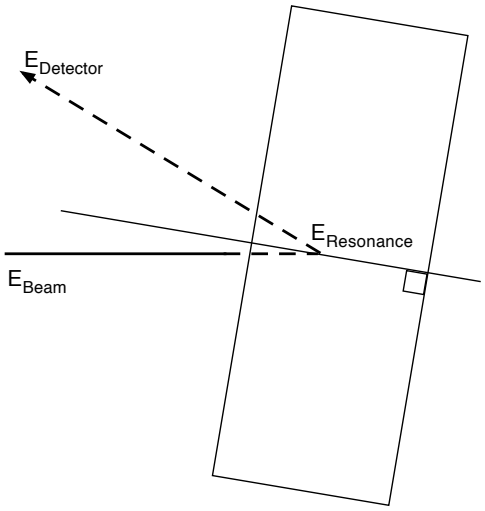

Figure 2.3: In the thick target backscattering technique the beam particles are slowed down inside the target material. Simulations using the material stopping power are needed to find the corresponding resonance energies.

The energy of an elastically scattered particle will then be detected with a value lower than the energy of the incident beam, but with the help of computer simulations and calculations of the stopping power in the material the interaction energy can be found and an excitation function constructed. To cover a large energy interval several steps must be taken, but they are limited in principle only by the energy of the first excited state in the target nucleus and can span several hundreds of keV, thus greatly reducing the beam time needed compared to the thin target technique. But due to straggling in the material and uncertainties in the simulations the resolution of the technique is limited. Details of the method can be found in [37] and in [38].

The thick black line in Figure 2.2 gives an example of an excitation function at 173° constructed from thick target backscattering data [20]. The data were taken using the K-20 cyclotron at Åbo Akademi University with a 10 μm thick plate of natural silicon as the target. The resolution is somewhat poorer than for the thin target data, but still all the major structures are clearly visible. In the experiment [20] data were taken at 21 angles between 107° and 173°, allowing a 3D plot of the cross section in the energy and angle plane as exemplified for

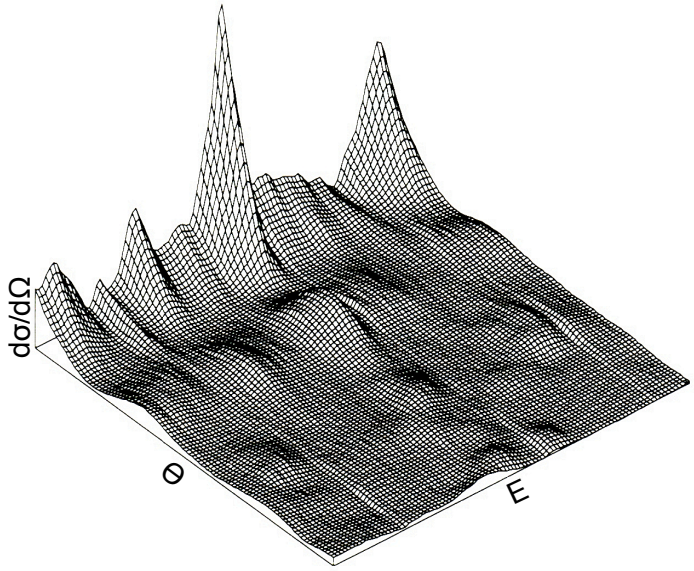

Figure 2.4: The cross section in the energy range 19.2–20.2 MeV excitation and the angle range 107°–173° in ^{32}S [20].

the energy range 19.2–20.2 MeV in Figure 2.4. The figure very nicely illustrates the characteristic squared Legendre polynomial behavior of the angular distribution expected for resonant scattering.

2.4 The Thick Target Inverse Kinematics Technique

Using inverse kinematics usually involves an accelerated heavy ion reacting with a gaseous target. This has several advantages:

- Gaseous and chemically unstable elements, that would be difficult or impossible to make into solid targets, can easily be used as beam ions.
- Very high purities can be reached in both the beam and the target, a clear advantage over using a solid target on a backing or a chemical compound solid target.

- The natural slowing down of a heavy ion in a thick target gas can be used to study all possible interaction energies in a single run.
- All scattered particles can be detected at forward angles, and if the gas pressure is adjusted to fully stop the beam inside the scattering chamber, scattered particles can also be detected at 0°. This corresponds to 180° in normal geometry and is impossible to obtain with backscattering because of the beam entering the scattering chamber at this angle.

The Thick Target Inverse Kinematics Technique (TTIK) was pioneered by V.Z. Goldberg at the Kurchatov Institute in Moscow, Russia [39]. A large part of the specialized software used has been developed by G.V. Rogachev [40, 41]. The technique has been used with modification at many institutions around the world and is discussed e.g. in the thesis of K.-M. Källman [38]. Some details of the method are given below through the example of the ^{28}Si + α reaction as used in PAPER 1. This reaction is of special interest since there exists detailed data from previous experiments which can be used for comparison.

2.5 An Example TTIK Setup

The K-130 cyclotron of the University of Jyväskylä in Finland [42] was used in the experiment. Figure 2.5 shows the experimental setup. Ions of ^{28}Si with a beam energy of 150 MeV entered the scattering chamber through a Havar foil, loosing about 15 MeV in the process. The scattering chamber used had an inner radius of 65 cm and featured six silicon surface barrier detectors, separated by 6°, mounted on a turntable with a radius of 55 cm. A seventh detector was mounted fixed at -15° for monitoring and calibration. The chamber was filled with helium gas at a pressure of 289 Torr and a temperature of 27.2° C. This provides a gas dense enough to completely stop the beam inside the chamber before the 0° detector. The maximum energy of scattered alpha-particles is about 70 MeV, and since the energy loss of these is more than 100 times

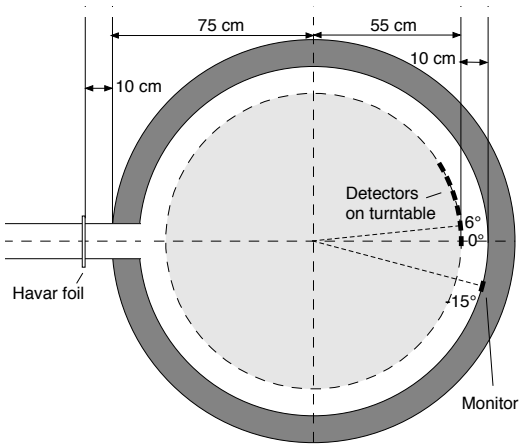

Figure 2.5: A typical TTIK setup with the detectors at forward angles.

smaller than for the ^{28}Si ions, the alpha-particles can travel almost undisturbed to the detectors. An advantage of the TTIK technique is the relative insensitivity to straggling of the beam, both in the entrance foil and in the gas filled chamber, details are given in [38].

The main disadvantage of the technique is the limited resolution, especially at low energies and high angles. There are several factors that contribute:

- Since scattering occurs along the whole of the beam path, and the detectors are all placed close to 0°, reactions at different distances from the detectors will correspond to different solid angles.

- The resolution for scattering occurring close to the entrance of the chamber is very good, but as the beam slows down there is more and more straggling of the heavy particles, giving poorer resolution at low energies.

- Because of the straggling, scattering events from a certain resonant state will occur at slightly different distances from the detectors. This does not noticeably affect the resolution at 0°, but the larger the angle, the more it broadens observed structures in the CM-spectra.

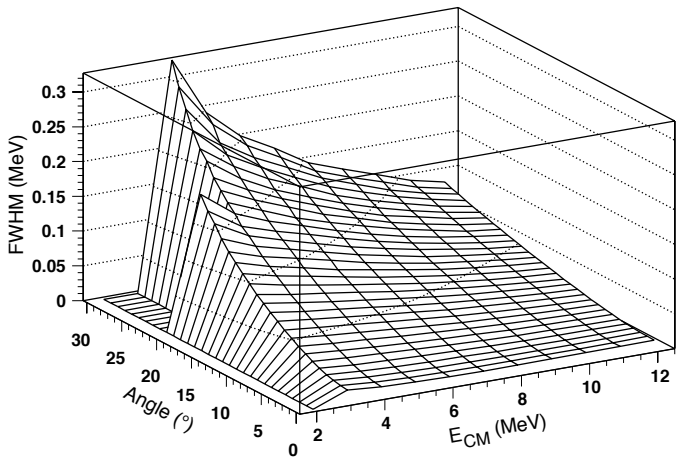

Figure 2.6: Resolution simulation for a TTIK experiment. Typically, the resolution improves with higher energies and lower angles.

The expected resolution can be simulated for specific experimental conditions, and such a plot for the ^{28}Si + α experiment is shown in Figure 2.6. The simulation can be used in the analysis phase for convolution of the theoretical curve.

The experimental setup in this case did not include any attempts of finding the parity of the resonances. It would be tempting to assume natural parity, giving positive parity for even spin levels and negative parity for odd spin levels, but to verify such an assumption would require a much more complicated setup and analysis.

In the example case the turntable was rotated so that each detector collected data at 8 different angles. After the experiment the best data set from a single detector was chosen for the analysis, as well as a set from a second detector for comparison. Some of the detector characteristics

Table 2.1: Detector characteristics. Data from the primary detector were used for the main analysis and data from the secondary for comparison. All detectors used a collimator with a diameter of 5 mm.

	D (mm)	A (mm^2)	Γ (keV)
Primary detector	2.0	50	17
Secondary detector	5.0	75	100

are given in Table 2.1. The data collected must be treated in several steps in order to be transferred to CM coordinates. This is done with a special computer code [40, 41].

2.6 Treatment of TTIK Data

The first step is to separate out protons and other similar unwanted events. Time-of-flight was measured using the RF signal from the cyclotron and the fast signal from the detectors. The measurement was limited by the relatively short distances inside the chamber, giving a time-of-flight for alpha-particles scattered close to the chamber enterance of about 20 ns. The overall time resolution was about 2.5 ns, which was good enough to extract alpha-particle events, but not enough to distinguish between elastic and inelastic events. The inability to separate elastic from inelastic events is one of the main limitations of the technique in the used setup. A more complete time-of-flight measurement would be preferable and has been performed using the same technique at other labs, e.g. [43].

Each event recorded by the detectors must be traced back to the point of interaction along the beam path. The CM energy can be calculated and the differences in solid angles depending on the distance from the detectors must be compensated for. The stopping powers for the heavy ion and the scattered particle in the target gas are usually simulated with software such as SRIM [44]. In experiments where the mass difference between the heavy beam ion and the target nucleus is small this gives rise to rather large errors and the stopping powers have to be measured experimentally. But in the case of ^{28}Si + α the uncertainties of the simulations do not limit the resolution of the experiment.

The example experiment did not have a separate setup for measuring the absolute cross section, but by fitting the Coulomb scattering part at low energies a calibration in very good agreement with previous values was obtained. An energy calibration of the detectors was performed with a ^{226}Ra source. The maximum energy of the emitted

alpha-particles from this source is 7.65 MeV, compared to the maximum alpha-particle energy recorded by the detectors of close to 70 MeV, making the energy calibration somewhat uncertain especially at high energies. Still, the CM-converted spectra corresponded very nicely to previous data, only needing a linear shift of -150 keV to coincide. It is unclear if this is due to uncertainties in the energy calibration of this or the previous experiments. Spectra taken at angles larger than 4° also needed to be scaled by a factor of about 0.9 in energy in order for the structures to coincide with the 0° spectrum and previous data.

It is important to note that the CM-spectra obtained with the TTIK technique cannot be directly compared over large energy intervals to spectra obtained through other techniques, because of the difference in laboratory angles. A spectrum for 180°, corresponding to 0° in inverse kinematics, cannot be obtained in traditional geometry, and for all other detector angles using the TTIK technique there is an energy dependence in the corresponding CM angle. This is because each detector detects particles emerging from collisions along the whole path of the beam. An alpha-particle scattered close to the entrance window will hit a detector fixed at a certain angle compared to the center of the chamber with high energy and correspond to a rather low laboratory angle. An alpha particle scattered close to the other end of the chamber will hit the same detector with low energy and correspond to a much larger laboratory angle. Figure 2.7 shows an example of the laboratory and CM angle dependency for a detector fixed at 12° compared to the center of the chamber in the example ^{28}Si + α experiment.

In Figure 2.2 the thin black line illustrates TTIK data. The resolution is somewhat poorer than for the other techniques illustrated in the same figure, but all the major structures can still be seen. There is an extra background in the TTIK data, mainly from inelastic events. The insert shows the same TTIK data as the black line, with the gray area representing the thin target data smoothed by 45 keV and with an extra background of 50 mb/sr added. The agreement is very good, and thus, one can conclude that the TTIK method produces reliable data detailed enough for further analysis.

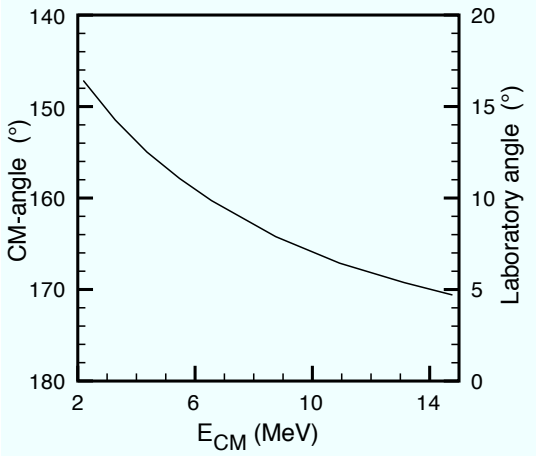

Figure 2.7: CM and laboratory angles depending on energy for a detector fixed at 12°.

2.7 Simplified R-matrix Analysis

After the conversion to the CM frame, the data taken with the TTIK technique was analyzed using a custom implementation of simplified R-matrix analysis [40, 45, 46]. For spinless particles the cross section can be separated in a non-resonant part and a sum of partial waves giving the standard expression:

$$\begin{aligned}\frac{d\sigma}{d\Omega} &= \mid f_C(\theta) + \rho(\theta)e^{i\chi} - \frac{i}{2k}\sum_m (2l_m+1) \\ &\quad \cdot\frac{\Gamma_{l_m}}{\Gamma}\cdot(e^{2i\beta_{l_m}}-1)\cdot e^{2i\phi_{l_m}}\cdot P_{l_m}(\cos\theta)\mid^2 . \end{aligned} \tag{2.1}$$

Here, $f_C(\theta)$ is the Coulomb scattering amplitude, and $\rho(\theta)$ and χ are the amplitude and phase shift of the background. The resonant phase shift β_l is given by

$$\beta_l = \arctan\left(\frac{\Gamma}{2(E_{res}-E)}\right) \tag{2.2}$$

and ϕ_l is a relative background phase shift. In the above equation $P_l(\cos\theta)$ is the Legendre polynomial of order l. For a single alpha-

particle resonance without background the cross section can be written:

$$\frac{d\sigma}{d\Omega} = \frac{(2l+1)^2}{k^2} \cdot \left(\frac{\Gamma_\alpha}{\Gamma}\right)^2 \cdot P_l^2(\cos\theta). \tag{2.3}$$

In the analyzing software resonances are added manually with four parameters: energy (E), spin (l), width (Γ) and strength (Γ_α/Γ). A phase shift parameter (ϕ_l) can also be used, but to simplify the analysis in the example case this value was assumed to be 0 in the present work. The coherent background was also put to 0, instead a non-coherent background was added manually for each angle, as a linear function of energy connecting points 1–2 MeV apart.

Based on the resonance parameters the software builds a theoretical excitation curve corresponding to each available detector angle as defined in the input files. The theoretical curve is convoluted with the simulated resolution (see Figure 2.6) in order to better correspond to the observed spectrum. More and more resonances are added and the parameters adjusted until a satisfactory fit for all the data is achieved.

The software also includes an automated fitting routine. But because of the large number of close-lying resonances and the many free parameters, it could only be used after a reasonable fit was first achieved manually. For spectra corresponding to different angles, the resonances did not line up perfectly because of small uncertainties in the calibrations and the conversion to CM. This meant that the automated fitting procedure could only be used on one spectrum at a time and could not be used for fitting the spin values of resonances. Although some energies and widths were fitted using the software routines, in practice the best fits were judged only by eye, trying to find the best fit encompassing all the available data.

The alpha-particle width Γ_α and the alpha-particle reduced width γ_α^2 are related through the formula

$$\Gamma_\alpha = 2P_l\gamma_\alpha^2, \tag{2.4}$$

where P_l now represents the penetrability factor. It can be calculated using

$$P_l = \frac{Rk}{F_l^2 + G_l^2}, \tag{2.5}$$

where $F_l(\eta, kR)$ and $G_l(\eta, kR)$ are the regular and irregular solutions for the Coulomb wave function, respectively, with the Sommerfeld parameter $\eta = \mu Z_1 Z_2 e^2 / 4\pi\epsilon_0 \hbar^2 k$, the wave number $k = \sqrt{2\mu E}/\hbar$ and the channel radius R.

The reduced alpha-particle width γ_α^2 is of great interest to calculate as it can be compared to the single particle limit

$$\gamma_{sp}^2 = \frac{\hbar^2}{\mu R}. \tag{2.6}$$

If the reduced width of a resonance is close to the single particle limit, it can be interpreted as a cluster state. In older literature the so called Wigner limit γ_W^2 is often used instead of the single particle limit, with $\gamma_W^2 = (3/2)\gamma_{sp}^2$.

It must be stressed that this method of analysis applied to present quality of experimental data is only approximate. In most cases the limited resolution only permits assignment of upper limits for widths and reduced widths. Also the spin assignments are somewhat uncertain. But comparison to previous data for ^{32}S shows that the gross features are reliably reproduced with the method, see Figure 2.8.

The most interesting results are not individual parameter assignments, but the general distribution of groups of resonances with different spin, their summed reduced widths, and the development of spins, widths, strengths and densities of the resonances with energy. All of these characteristics can be reliably discussed based on the new data presented in this thesis and in the appended PAPERS. This despite the limitations of the experimental method of elastic scattering, the experimental technique of thick-target inverse kinematics, the resolution of the acquired data and the simplified R-matrix method of analysis.

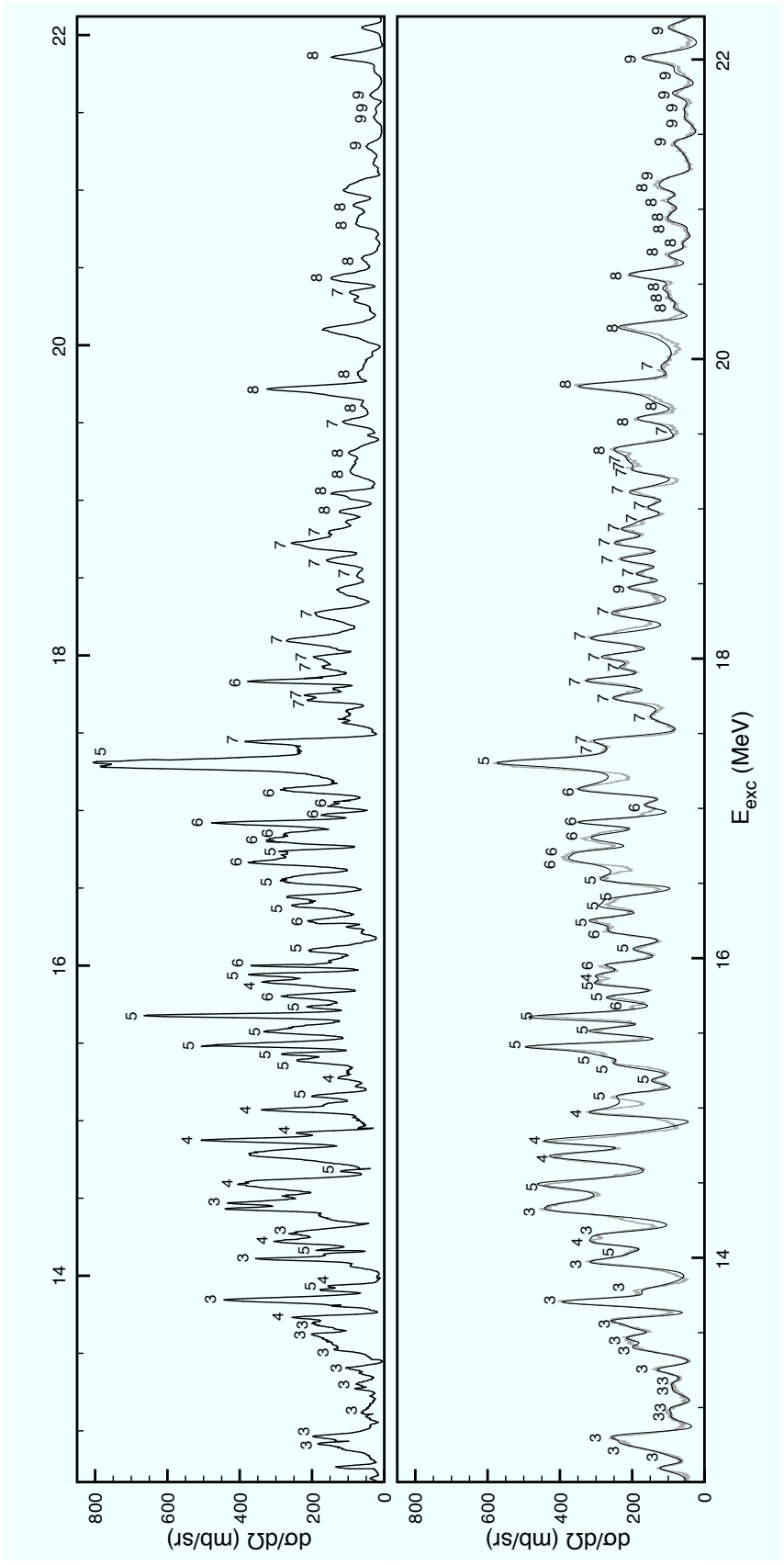

Figure 2.8: Comparison of new TTIK data for ^{32}S (bottom panel) with previous thick target data (top panel) [20]. The numbers above the resonances represent the fitted spins. In the bottom panel the experimental data is shown in gray and the black line represents the fitted curve. The thick target data in the top panel was taken at 174° CM, while the TTIK data was recorded by a detector at 2°, corresponding to CM angles 174°–178° depending on the energy.

In Figure 2.9 the subtle differences between fitting individual resonances with alternative sets of parameters are illustrated. The variation between different possibilities are not large, but still clear enough to make probable assignments. In Figure 2.10 another example is given, showing the much clearer difference between alternatives when fitting a whole group of resonances and taking a larger region into account.

2.8 Transfer Reactions

A different method of studying resonances is through transfer reactions. For studying alpha-particle resonances it is suitable to use a ^{6}Li beam, since this nucleus easily dissolvs into an alpha-particle and a deuteron, leading to a break up reaction ($^6\mathrm{Li} \rightarrow \alpha + d$). The setup for this kind of experiment is a bit more complicated, since it involves the detection of deuterons at forward angles in coincidence with alpha particles at backward angles, in both cases needing particle telescopes or well calibrated position sensitive detectors to separate out unwanted events. On the other hand transfer reactions do not have the same restrictions regarding detection of high spin resonances at low energies as imposed by penetrability factors on elastic scattering experiments, as discussed in Section 3.1.

Such an experiment has been performed with success for the reaction ^{28}Si(^{6}Li,d)$^{32}\mathrm{S}^* \rightarrow \alpha$ + ^{28}Si, examining highly excited possible alpha-cluster states at 24–36 MeV excitation energy in ^{32}S [21]. The authors of the report found a surprisingly strong correlation between the deuterons detected at forward angles and alpha-particles at backward angles. Strong resonances were observed even though the resolution of the experiment was only a few hundred keV. It was also possible to study correlations between events in the elastic, first inelastic and second inelastic channels. The disappearance of elastic cross section at about 31 MeV for this reaction, discussed in e.g. PAPER 5, was confirmed, together with increased cross sections in the inelastic channels at about the same threshold energy.

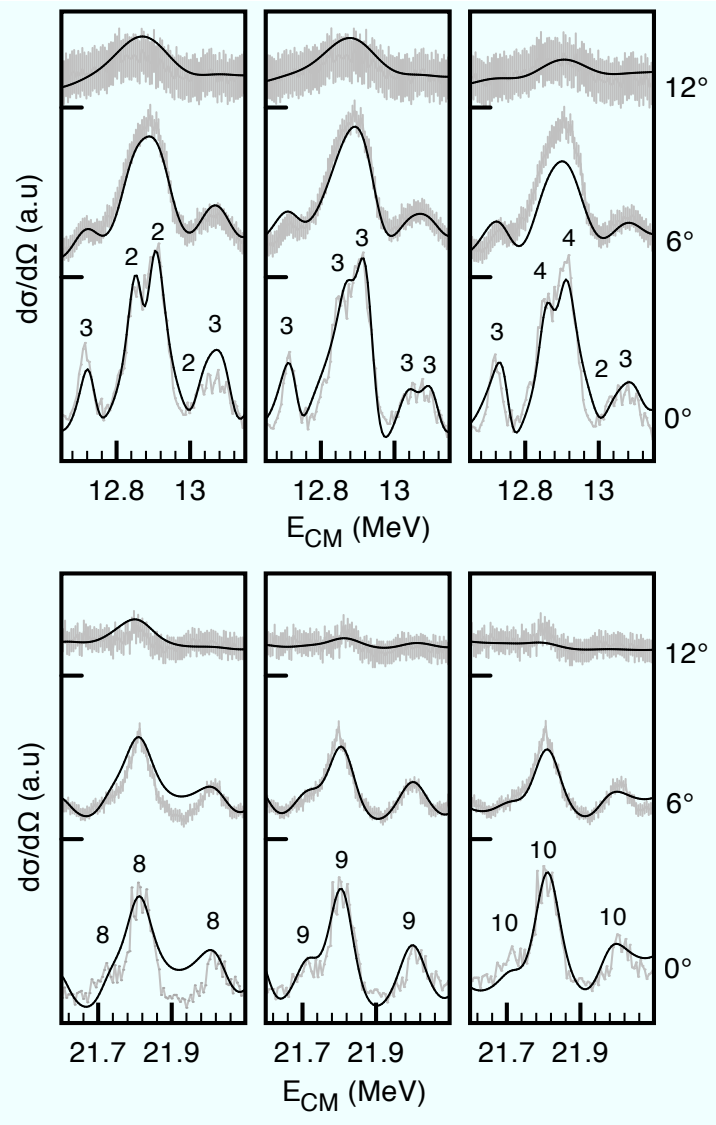

Figure 2.9: Examples of different fits for the regions around 12.9 MeV (top) and 21.8 MeV (bottom) in ^{32}S. The experimental data are given in gray. The bottom, center and top black curves in each panel show the fits for the data from the detectors at 0°, 6° and 12° respectively and the spin values used are indicated above the 0° spectrum. The center panels represent the best fits, as judged by the author.

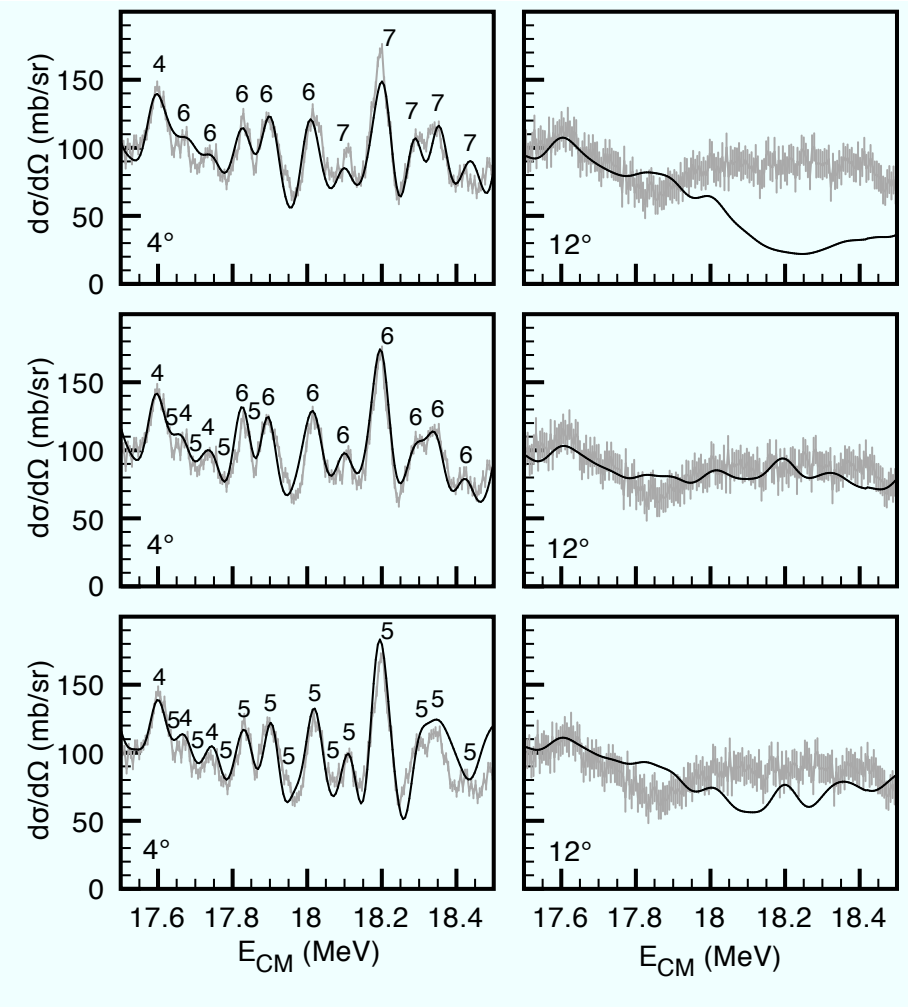

Figure 2.10: Examples of fitting an entire region with different spin parameters in ^{34}S. Again the experimental data is given in gray with the black lines representing the fits corresponding to the spin values indicated in the left panels. As can be seen, the structures at one angle (e.g. 4°) can be fitted in several different ways, but the data at other angles, here only represented by the 12° spectrum, help determine the most probable fit. In this case the best fit is dominated by spin 6 resonances as shown in the center panels.

Chapter 3

Experimental Results

3.1 Main Results for ^{32}S

The TTIK data for the reaction ^{28}Si + α, populating highly excited states in ^{32}S, was fitted with a total of 129 resonances in the excitation energy range 10–24 MeV in ^{32}S. Full details on the experimental setup and resonance parameters can be found in PAPER 1. Figure 3.1 shows some examples of the resulting fits.

The results were compared to previous values reported in [20, 38, 22], in order to validate the method and, if possible, confirm and expand on previous resonance parameter assignments. In Figure 2.8 a selected region of the TTIK data (bottom panel) is compared to data from [20]. As can be seen, the same structures are seen in both sets, and the spin assignments indicated above each resonance correspond very nicely.

It is interesting to plot the energies of the observed levels with respect to $l(l+1)$, as shown in Figure 3.2. The diamonds represent an average energy for each spin value, weighted with the reduced widths of the individual resonances. The levels closely follow a straight line, indicating a quantum mechanical rotor. The extracted moment of inertia J, using the formula

$$E_{exc} = E_0 + \frac{\hbar^2}{2J} l(l+1),$$

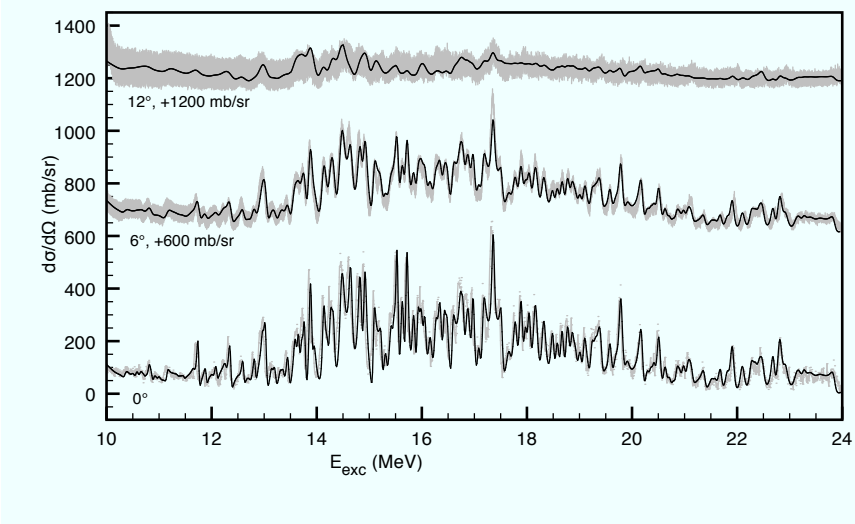

Figure 3.1: Examples of the fits for ^{32}S for selected angles. The gray line shows the experimental data including uncertainties, while the black line represents the fitted curve.

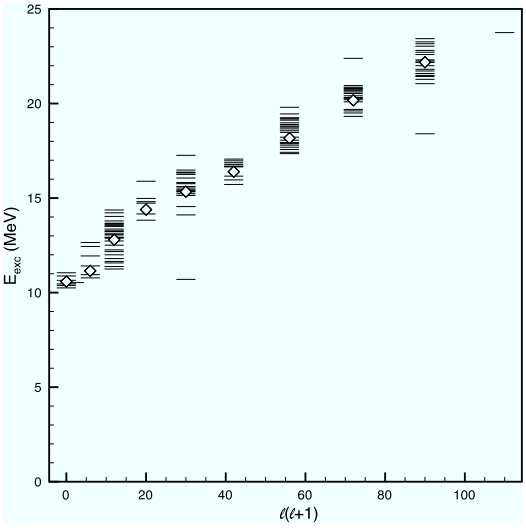

Figure 3.2: Resonances in ^{32}S plotted according to their energies and $l(l+1)$. The diamonds represent weighted averages.

is 3.9 $\pm$ 0.3 $\hbar^2$/MeV. This is much lower than the value of 5.3 $\hbar^2$/MeV for a rotating ^{32}S sphere, and much higher than the value 2.8 $\hbar^2$/MeV for an alpha-particle orbiting a ^{28}Si core. An interpretation is that this represents a configuration where a few alpha-particles orbit an inert core partly submerged in the surface, or possibly a surface wave. The alpha cluster levels are fragmented on many narrow resonances, but the summed reduced widths for each spin are comparable with the single particle limit.

An important limitation of the experiment is the fact that at low energies high-spin resonances are expected to be very narrow and might not be observed among strong low-spin structures. The cross section can be estimated using Equation 2.3 convoluted with the experimental resolution. These calculations show that the observation of a certain spin usually begins a few MeV above the theoretical lower limit of observation, and so do not affect the reliability of the results.

3.2 Main Results for ^{34}S

While the ^{32}S nucleus is well examined from elastic alpha-particle scattering point of view, there is very little previous data on ^{34}S. Earlier examinations have concentrated on finding optical potential parameters for ^{34}S, and only one reference showing a continuous excitation function could be found [47]. The data could be used for checking the calibration of energy and cross section, but in the reference no attempts at making resonance parameter assignments were made.

The same setup as in the previous experiment was used and the details are found in PAPER 2. A total number of 111 resonances, between 12 and 24 MeV excitation energy, were added in the fit shown in Figure 3.3. The dashed lines in the bottom panel illustrate some of the theoretical limits of observation for selected spin values. As for ^{32}S the observation of a certain spin value usually begins at least one MeV above the lower limit, except for spin 2 resonances, where observation of resonances coincide with the limit.

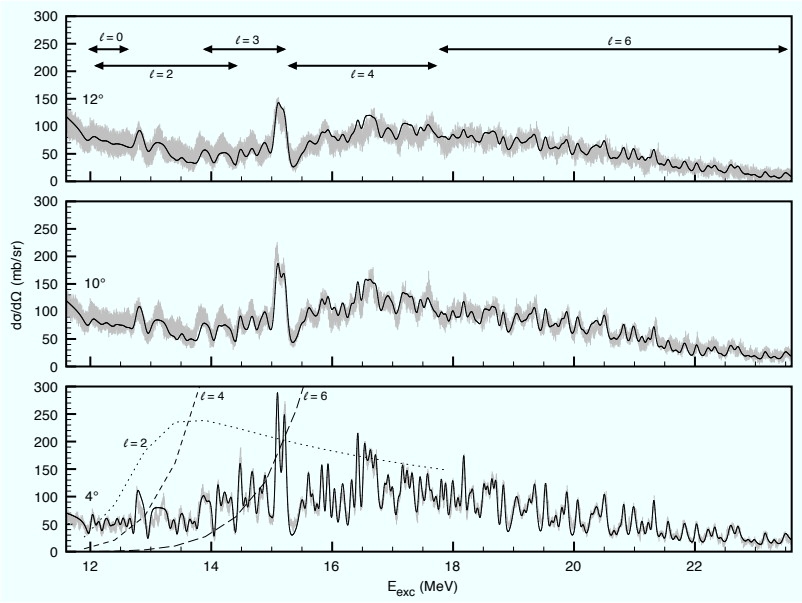

Figure 3.3: Examples of the fits for ^{34}S. The regions where certain spin values are found are indicated with arrows in the top panel. The dashed lines in the bottom panel shows examples of theoretical limits of observation for some spin values.

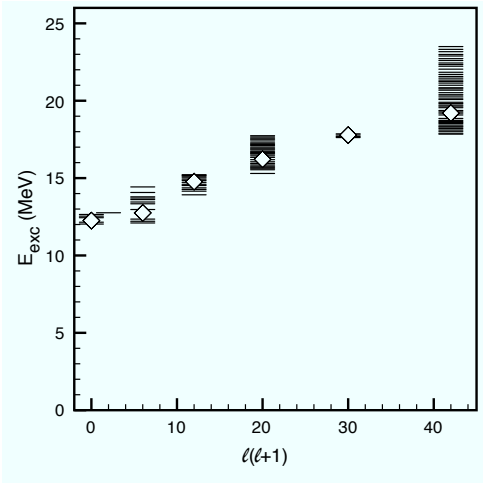

Figure 3.4: The plot of energy versus $l(l+1)$ for ^{34}S also shows a linear behavior but corresponding to a smaller value of J compared to ^{32}S.

Again the energy versus $l(l+1)$ plot shown in Figure 3.4 is interesting. The groups of resonances line up in the same way as for ^{32}S but the slope is clearly different. The value for J is 2.9$\pm$0.3 $\hbar^2$/MeV, coinciding with the value of 2.9 $\hbar^2$/MeV for an alpha-particle orbiting a ^{30}Si core at touching distance. The linear dependency in the plot still indicates a rotational behavior, but the surface rotation involves a clearly smaller mass. The cross section is also roughly halved compared to ^{32}S, probably due mainly to the difference in neutron separation energy.

3.3 Main Results for ^{40}Ca

The doubly magic ^{40}Ca nucleus has been well examined in many different experiments, but again mostly for optical potential calculations. Excitation functions were measured in a detailed experiment by Wallace et al. in 1970 [30]. Unfortunately the rich structures in the data were only averaged to examine the optical potential. But there was a partial overlap in energy between the raw spectra from [30] and those from the present experiment, and some of the structures could be identified in both data sets and used for checking the calibrations.

For the present experiment the same setup as in the two previous measurements was used, and the full details can be found in PAPER 3. An impressive 137 resonances were added to the fit between 12 and 20 MeV excitation energy in ^{40}Ca, see Figure 3.5. This density of resonances is roughly twice as large as that of ^{32}S and ^{34}S.

The energy versus $l(l+1)$ plot is shown in Figure 3.6. The value for J becomes 3.8$\pm$0.3 $\hbar^2$/MeV, very close to that of ^{32}S, but since ^{40}Ca has a larger radius, the mass involved in the rotation is slightly smaller than for ^{32}S.

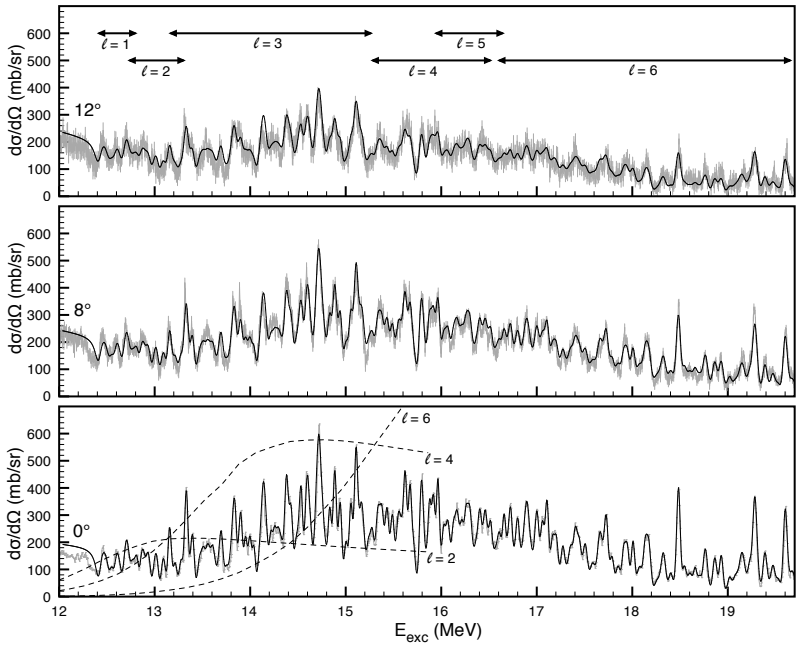

Figure 3.5: Examples of the fits for ^{40}Ca. Again the regions where certain spin values are found are indicated with arrows in the top panel. The dashed lines in the bottom panel shows examples of theoretical limits of observation for some spin values.

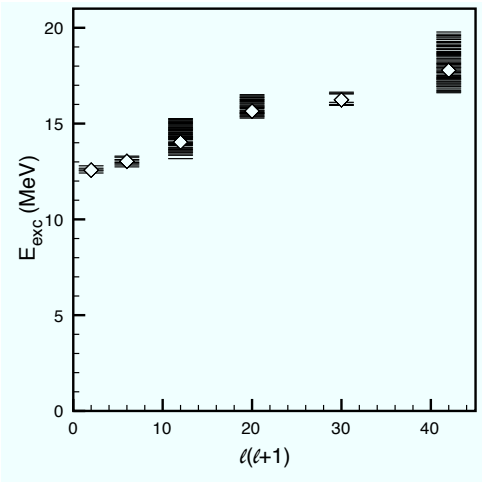

Figure 3.6: Energy versus $l(l+1)$ for ^{40}Ca. Again a linear behavour is observed, with a value of J similar to that of ^{32}S.

3.4 Comparison of Results for ^{32}S, ^{34}S and ^{40}Ca

In Figure 3.7 low-angle spectra for all the nuclei are compared. The general appearance is surprisingly similar, but there are also clear differences. Some values are compared in Table 3.1 and more details are given in PAPERS 3 and 4. The most striking similarity is the rich structure with many narrow peaks and a maximum cross section at about 16 MeV in excitation energy. For all the nuclei the narrowest observed resonances correspond to a lifetime of more than 100 transit times, implying that some form of fusion takes place, but there is not enough time for thermalization. Using the TTIK technique, it is expected to have better resolution for heavier beam particles, but the effect does not completely explain the half as narrow peaks observed in ^{40}Ca compared to ^{32}S and ^{34}S. The density of resonances is also twice as high in ^{40}Ca. The cross sections for ^{32}S and ^{40}Ca are very similar, but for ^{34}S it is only about half of that of the self-conjugate nuclei.

For all the nuclei the summed relative reduced widths for resonances of the same spin are clearly over-estimated. But for all the nuclei the sums are of the same order as the single particle limit, giving credibility to the interpretation of the observed structure as rotational levels split into many close-lying resonances. It is also interesting to note that the average summed relative reduced widths for ^{32}S and ^{40}Ca are very similar, while the average for ^{34}S is only one third as large.

Table 3.1: Comparison of some values.

	^{32}S	^{34}S	^{40}Ca
Resonances / MeV	9.1	9.7	18.6
Mean widths (keV)	69	56	31
Max. cross section (mb/sr)	~ 600	~ 300	~ 600
Moment of inertia ($\hbar^2$/MeV)	~ 3.9	~ 2.9	~ 3.8
Average $\sum \frac{\gamma_\alpha^2}{\gamma_{sp}^2}$ (%)	< 207	< 72	< 227
Q_α (MeV)	-6.95	-7.92	-7.04
S_n (MeV)	15.04	11.42	15.64
S_p (MeV)	8.86	10.88	8.33

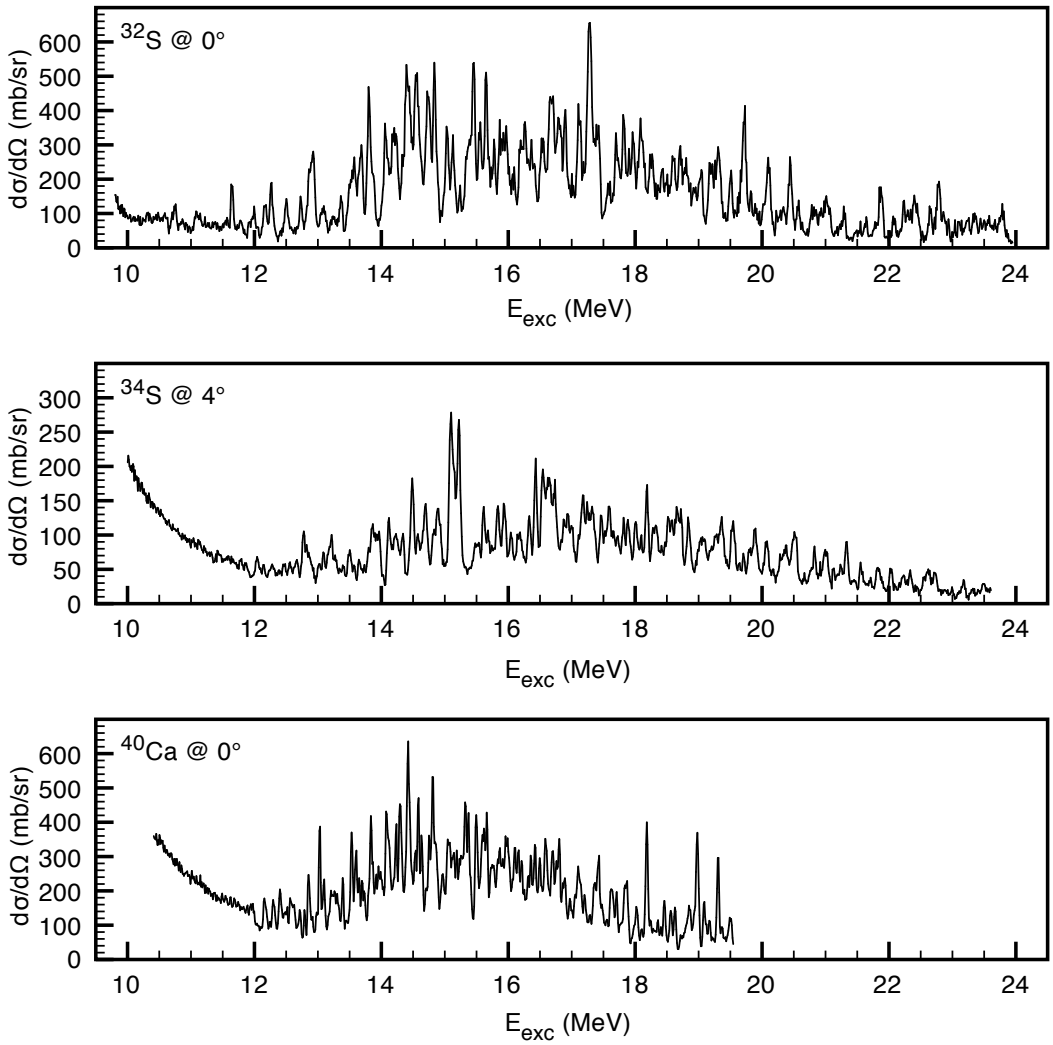

Figure 3.7: Comparison of spectra for ^{32}S, ^{34}S and ^{40}Ca.

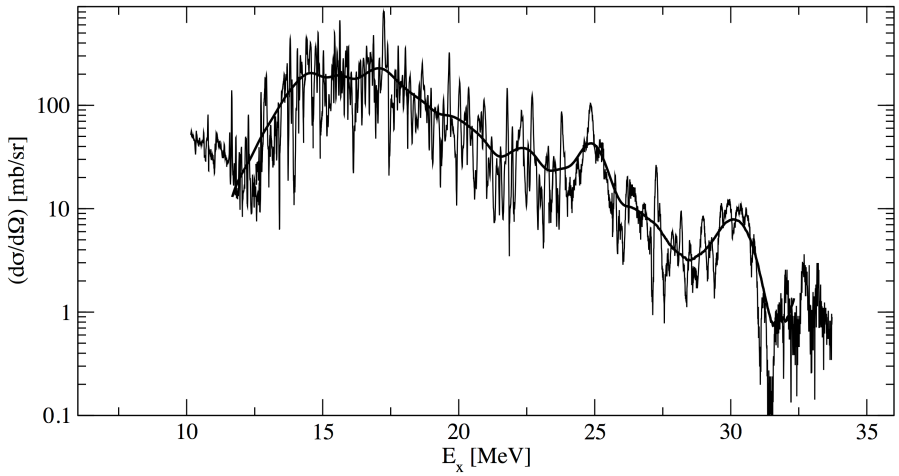

Figure 3.8: Logarithmic plot of ^{32}S (see PAPER 5), showing a clear decrease in cross section at threshold values 25 MeV and 32 MeV excitation energy. After 32 MeV the cross section is almost zero and no further clear structures are observed.

The extracted moments of inertia are again quite similar, but when considering the different radii of the nuclei, the value for ^{34}S is very close to that of one orbiting alpha-particle, while the values for ^{32}S and ^{40}Ca both correspond to 2–3 orbiting alpha-particles. The reason for this and its interpretation are unclear.

In Figure 3.8 a logarithmic plot of the most complete excitation function for this nucleus is shown, and it is discussed in more detail in PAPER 5 and in [23]. There are two especially interesting broad enhancements of cross section followed by a sharp decrease at about 25 MeV and 32 MeV. After the latter the cross section falls to almost zero. Interestingly these energies roughly coincide with the threshold energies of break up into a core plus 3 or 4 alpha-particles, respectively.

The interpretation of this is also unclear, especially since the angular momenta observed at high energies are very large, giving a high angular momentum barrier effectively preventing simple evaporation of the alpha particles from the surface. In the transfer experiment [21] an enhancement in the inelastic channels was observed at the 32 MeV drop off of elastic cross section. There is an interesting similarity to this disappearance of cross section in the excitation function for ^{40}Ca

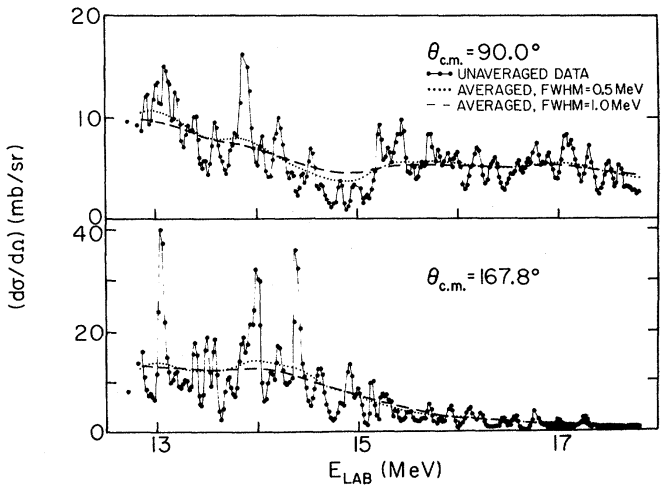

Figure 3.9: High energy excitation function for ^{40}Ca from [30]. The final large peak in the bottom panel spectrum at about 14.5 MeV laboratory energy can be identified as the last fitted resonance at 19.78 MeV excitation energy in Figure 3.5. Note the rapid decrease in cross section and lack of structure after 15.5 MeV laboratory energy, corresponding to the break up energy of ^{40}Ca into ^{28}Si and three α-particles at 20.6 MeV excitation.

found in [30] (Figure 3.9), where it is seen that the final resonance reported in PAPER 3 at 19.78 MeV is indeed the last major structure, for energies higher than this only very minor peaks are observed. This can be compared to the break up energy of ^{40}Ca into ^{28}Si and three α-particles at 20.6 MeV.

A TTIK experiment has also examined ^{36}Ar in a very similar manner [29]. There only the low energy region of 12–16 MeV excitation energy was analyzed in detail with the simplified R-matrix approach, but the results are similar to the ones presented in this thesis, with the stronger resonances lining up in an energy versus $l(l+1)$ plot and giving a moment of inertia for the rotational motion of about 6.8 $\hbar^2$/MeV, a value clearly larger than for the three nuclei examined in this thesis. A comparison of these are shown in Figure 3.10 and discussed more in detail in PAPER 3. Even though the moments of inertia differ in all four cases they have the clear rotational behavior in common.

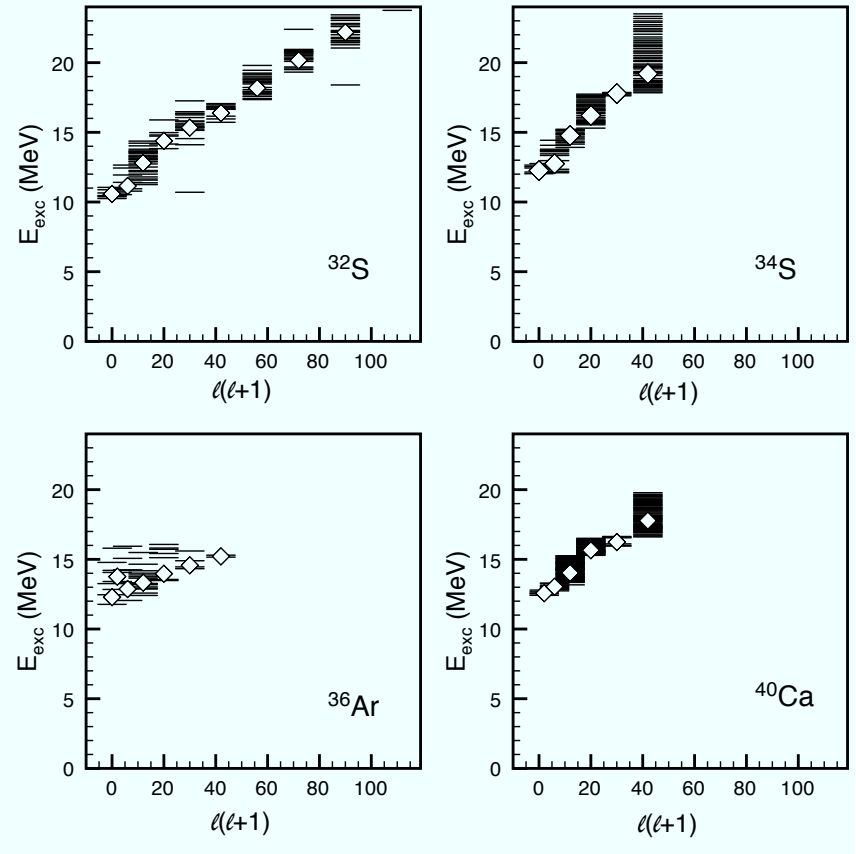

Figure 3.10: Comparison of excitation energy versus $l(l+1)$ for some medium light nuclei. The diamonds represent averages for different spin values weighted with the reduced widths of individual resonances. In all cases a linear behavior is observed, indicative of a quantum mechanical rotation.

3.5 Statistical Fluctuations

It is important to examine whether the very rich structure observed in the above experiments indeed comes from real resonances or just statistical fluctuations, as exemplified in Figure 3.11 from [48]. There are two forms of statistical fluctuations that might influence measurements at high excitation and give rich random structure to a spectrum [49]:

1. Porter-Thomas fluctuations appear for narrow resonances, when the experimental resolution is of the same order of magnitude as, or worse than, the spacing between resonances.

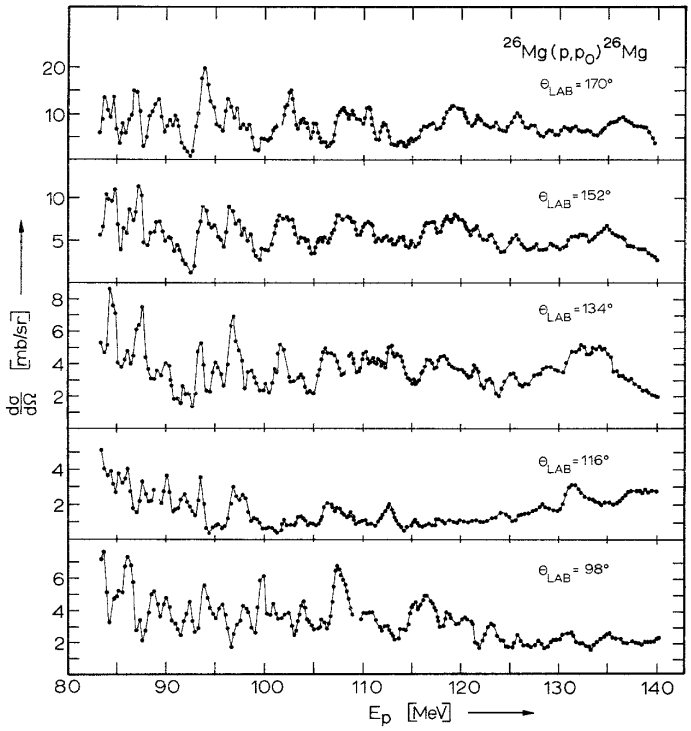

Figure 3.11: Examples of excitation functions where the structures were found to be mainly due to statistical fluctuations [48].

2. Ericsson fluctuations appear at high excitation where many open reaction channels are present, and the spacing between resonances becomes smaller than the widths of the resonances.

The Porter-Thomas fluctuations can be argued against since the results for ^{32}S are very similar to results from other high resolution studies (e.g. [19]). Even though the resolution of the TTIK experiments presented here is comparable to the spacing between the observed resonances, the same structures have been observed in other studies with much better resolution (see Figure 2.2) and must therefore be real.

Regarding Ericsson fluctuations the situation is more complicated, since the actual level density in the region is not precisely known. In [50] it is argued, again based on the high resolution study [19], that there are three signatures of cluster states:

- A cluster state appears as one or several strong resonances (compare the cross section of several hundred mb in Figure 3.1 with the few mb in Figure 3.11).
- It should be possible to extract a clear spin value for the resonances.
- The large peaks should be accompanied by minor peaks of the same spin, resulting from interference between the resonances and the statistical background. These were seen in the high resolution data as shoulders or separate small peaks close to the base of the strong peaks. But in the present data the resolution is not good enough to see this, instead the main resonance and the weaker fluctuation peaks melt together to form broadened peaks.

Therefore it can be concluded that it is likely that the structures presented in this thesis are real resonances.

Chapter 4

Summary and Discussion

In this thesis some recent discoveries regarding alpha-clusters among medium light nuclei have been discussed, and an attempt has been made to put these findings in the context of more general nuclear clusterization. The results from ^{32}S, ^{34}S and ^{40}Ca show the existence of levels with strong alpha-cluster properties at very high excitation in all of these nuclei, with the levels split into many close lying resonances and corresponding to a rotational motion on or in the nuclear surface. These results explore a mass region where relatively little is known about clusterization, and might hopefully some day contribute to bridging the gap of understanding between the light nuclei, where strong cluster aspects can be found at low excitation or even in the ground state, and the heavy nuclei where alpha-decay is still not completely understood and where heavy clusters are important.

A lot of development is going on in this field at the moment, both theoretical and experimental. One forefront is the use of various kinds of *ab initio* models, limited to light nuclei because of the complicated calculations and by our poor understanding of the nucleonic interactions. Another forefront is the development of new experimental methods, especially the use of radioactive beam facilities, which have made it possible to examine very exotic nuclear systems. But despite the present focus in the community on light nuclei and very exotic ones, much work still needs to be done among the stable medium-light nuclei. The results

presented in this thesis are not easy to interpret microscopically and many new questions are raised. There is a clear need for improved theoretical models for clusterization in these systems. And there are many nuclei for which no data at all are available, where there is a clear need for systematic large scale experimental investigations similar to the ones described in the chapters above.

Especially interesting and difficult to interpret are the extracted moments of inertia for the examined nuclei. What is clear is that the interpretation of a quantum mechanical rotor implies a surface effect, where a few alpha-particles on or in the nuclear surface orbit an inert core. At high excitation very high moments of inertia are observed, still the linear behavior of the moment of inertia remains and implies that no further deformation is taking place, until the resonances disappear at very high energy.

Even though the parity of the resonances was not measured experimentally it would, as stated in Section 2.5, be tempting to assume positive parity for even spin levels and negative parity for odd spin levels. Usually positive and negative parity bands are split up but here they are observed on the same line, maybe hinting at a picture of independent bosons interacting, maybe even in some form of Bose-Einstein condensate. Also the splitting of the levels into so many close lying resonances is difficult to explain, but an attempt can be made by viewing the surface effect as a quantum mechanical vortex [50].

The scientific community is increasingly financed via projects. Trends and buzzwords seem to be ever more important when competing for funding, and this naturally affects nuclear physics research as well. But let us hope that there is still room for basic research on stable nuclei, in the era of high-energy colliders and exotic radioactive beam facilities.

This is the nature of science: it must be carried out on all fronts simultaneously, as one never knows where the next break-through will be made.

Bibliography

[1] J. P. Vary. Acta Phys. Pol. B **42** 3-4, 397 (2011).

[2] M. A. Khaleel (editor). *Scientific Grand Challenges: Forefront Questions in Nuclear Science and the Role of High Performance Computing* (U.S. Department of Energy Technical Report, 2009). doi:10.2172/968204.

[3] D. J. Rowe. *Nuclear collective motion. Models and theory.* (Hackensack, NJ: World Scientific, 2010).

[4] M. Freer. Reports on Progress in Physics **70** 12, 2149 (2007).

[5] C. Beck (editor). *Clusters in nuclei, Volume 1*, volume 818 of *Lecture Notes in Physics* (Springer Berlin / Heidelberg, 2010). doi: 10.1007/978-3-642-13899-7.

[6] M. Brenner (editor). *Cluster Structure of Atomic Nuclei* (Research Signpost, 2010).

[7] D. S. Delion (editor). *Theory of Particle and Cluster Emission*, volume 819 of *Lecture Notes in Physics* (Springer Berlin / Heidelberg, 2010). doi:10.1007/978-3-642-14406-6.

[8] G. Gamow. Z. Phys. A **51**, 204 (1928). doi:10.1007/BF01343196.

[9] L. R. Hafstad and E. Teller. Phys. Rev. **54** 9, 681 (1938). doi:10.1103/PhysRev.54.681.

[10] K. Ikeda, N. Takigawa and H. Horiuchi. Prog. Theor. Phys. Suppl. **E68**, 464 (1968). doi:10.1143/PTPS.E68.464.

[11] M. Freer. http://www.scholarpedia.org/article/Clusters_in_nuclei (Last checked August 2011). doi:10.4249/scholarpedia.9652.

[12] von Oertzen, W. *et al.* Eur. Phys. J. A **43** 1, 17 (2010). doi:10.1140/epja/i2009-10894-2.

[13] M. Chernykh *et al.* Phys. Rev. Lett. **98** 3, 032501 (2007). doi:10.1103/PhysRevLett.98.032501.

[14] Y. Funaki *et al. Alpha-particle condensation in nuclear systems*, 1. Cluster Structure of Atomic Nuclei (Research Signpost, 2010).

[15] V. Z. Goldberg *et al.* Phys. At. Nucl. **60** 7, 1061 (1997).

[16] A. S. B. Tariq *et al.* Phys. Rev. C **59** 5, 2558 (1999). doi:10.1103/PhysRevC.59.2558.

[17] V. Z. Goldberg *et al.* Phys. Rev. C **69** 2, 024602 (2004). doi:10.1103/PhysRevC.69.024602.

[18] S. Torilov *et al.* JETP Letters **94**, 6 (2011). doi:10.1134/S0021364011130170.

[19] M. Brenner *et al.* Acta Phys. Hung. N.S. **11**, 221 (2000).

[20] K.-M. Källman *et al.* Eur. Phys. J. A **16**, 159 (2003). doi:10.1140/epja/i2000-10158-9.

[21] M. Brenner *et al.* Physica Scripta **74** 6, 692 (2006). doi:10.1088/0031-8949/74/6/016.

[22] K.-M. Källman. Z. Phys. A **356** 3, 287 (1996). doi:10.1007/s002180050181.

[23] T. Lönnroth *et al.* J. Phys. G **38** 3, 035107 (2011). doi:10.1088/0954-3899/38/3/035107.

[24] S. Ohkubo and K. Yamashita. Phys. Rev. C **66** 2, 021301 (2002). doi:10.1103/PhysRevC.66.021301.

[25] M. Kimura and H. Horiuchi. Phys. Rev. C **69** 5, 051304 (2004). doi:10.1103/PhysRevC.69.051304.

[26] G. Kocak *et al.* Phys. Rev. C **81** 2, 024615 (2010). doi:10.1103/PhysRevC.81.024615.

[27] C. E. Svensson *et al.* Phys. Rev. Lett. **85** 13, 2693 (2000). doi:10.1103/PhysRevLett.85.2693.

[28] E. Ideguchi *et al.* Phys. Rev. Lett. **87** 22, 222501 (2001). doi:10.1103/PhysRevLett.87.222501.

[29] V. Z. Goldberg *et al.* Physics of Atomic Nuclei **63** 9, 1518 (2000). doi:10.1134/1.1312885.

[30] W. J. Wallace, K. R. Knuth and R. H. Davis. Phys. Rev. C **2** 5, 1738 (1970). doi:10.1103/PhysRevC.2.1738.

[31] D. Frekers, R. Santo and K. Langanke. Nuclear Physics A **394** 1-2, 189 (1983). doi:10.1016/0375-9474(83)90169-0.

[32] T. Yamaya *et al.* Phys. Rev. C **53** 1, 131 (1996). doi:10.1103/PhysRevC.53.131.

[33] A. A. Ogloblin. Int. J. Mod. Phys. E **17** 10, 2140 (2008). doi:10.1142/S0218301308011239.

[34] W. Gudowski. Acta Phys. Pol. B **31** 1, 107 (2000).

[35] V. Zagrebaev and W. Greiner. Int. J. Mod. Phys. E **17** 10, 2199 (2008). doi:10.1142/S0218301308011343.

[36] W. Greiner and D. N. Poenaru. *Neutron rich long-lived superheavies*, 119. Cluster Structure of Atomic Nuclei (Research Signpost, 2010).

[37] K.-M. Källman *et al.* Nucl. Instr. Meth. Phys. Res. **A338**, 413 (1994). doi:10.1016/0168-9002(94)91324-2.

[38] K.-M. Källman. *New Methods of Studying alpha-particle Resonance Scattering*. Ph.D. thesis, Department of Physics, Åbo Akademi University (1998).

[39] V. Z. Goldberg and A. E. Pakhomov. Phys. At. Nucl. **56**, 1167 (1993).

[40] G. V. Rogachev. *Simplified R-matrix code for spinless particles* (1999, unpublished).

[41] G. V. Rogachev *et al.* AIP Conf. Proc. **1213**, 137 (2010). doi:10.1063/1.3362563.

[42] E. Liukkonen. *New Cyclotron at Jyväskylä*, 22. Proceedings of the 13th International Conference on Cyclotrons and their Applications: Vancouver, BC, Canada, 6-10 July 1992 (World Scientific Publishing Co., Singapore, 1992).

[43] M. G. Pellegriti *et al.* Journal of Physics: Conference Series **267** 1, 012011 (2011).

[44] http://www.srim.org (Last checked August 2011).

[45] S. R. Riedhauser. Phys. Rev. C **29** 6, 1961 (1984). doi:10.1103/PhysRevC.29.1961.

[46] C. A. Davis and R. Abegg. Nucl. Phys. A **571**, 256 (1994). doi:10.1016/0375-9474(94)90061-2.

[47] P. Manngård. *Experimental Search for Alpha-Cluster States in Mid sd-Shell Nuclei*. Ph.D. thesis, Åbo Akademi University (1996).

[48] O. Häusser *et al.* Nuclear Physics A **109** 2, 329 (1968). doi:10.1016/0375-9474(68)90597-6.

[49] E. Grosse. http://www.efnudat.eu/IRMM_Workshop/Wednesday/2904_1130_Grosse.pdf (Last checked August 2011).

[50] M. Brenner and K. A. Gridnev. *Cluster states of a core plus alpha particles at high energies*, 43. Cluster Structure of Atomic Nuclei (Research Signpost, 2010).